

Thermochemical energy storage for cabin heating in battery powered electric vehicles

Megan Wilks^a, Chenjue Wang^a, Janie Ling-Chin^a, Xiaolin Wang^b, Huashan Bao^{a,*}

^a Durham University, Department of Engineering, Durham DH1 3LE, UK

^b Research School of Electrical, Energy and Materials Engineering, The Australian National University, Canberra, ACT 2601, Australia

ARTICLE INFO

Keywords:

Thermochemical adsorption
Thermal energy storage
Battery electric vehicle
Cabin heating
Dynamic performance

ABSTRACT

The potential of thermochemical adsorption heat storage technology for battery electric vehicle (EV) cabin heating was explored in this study. A novel modular reactor with multiple adsorption units was designed with working pair $\text{SrCl}_2\text{-NH}_3$. Numerical models of the proposed system were built, and the system was sized to meet the heating requirement for ambient temperatures ranging from -5 – 10 °C for 1 ~ 2 h. The simulation results showed the system can satisfy the required supply air temperature by initially activating 6 adsorption units and activating new units once detecting lower air temperature than required. It was found that the final global conversion of adsorption reaction was 0.62–0.67, indicating a relatively stable system performance over ambient temperatures. To supply a heating power of 1.3 kW for 1 h at an ambient temperature of 5 °C, the designed storage system had an adsorbent mass of 16.37 kg in 12 adsorption units. More adsorption units were needed for lower ambient temperatures, such as 23 adsorption units needed to supply a heating power of 2.4 kW at -5 °C ambient condition. It was found that the overall system energy density was 73.8 kWh/m³, whereas the material energy density was 169.4 kWh/m³. This work also demonstrates the importance of considering adsorption dynamics when assessing the performance of an adsorption system and demonstrates the benefits of a modularly designed adsorption reactor for cabin heating.

1. Introduction

The transition to electric passenger vehicles will play a crucial element in decarbonising the transport sector, with several countries, such as the UK, having recently brought forward a ban on sales of new fossil-fuelled vehicles to 2030 [1]. However, concerns about range variability depending on climate and high vehicle costs remain barriers to the uptake of battery electric vehicles (EVs). Reducing vehicle energy consumption to improve driving range or reduce battery capacity requirements remains an essential field of research.

When electric motors replacing internal combustion engines (ICEs) are entirely powered by onboard batteries, the limited battery capacity reduces the driving distance of EVs. In cold climates, the absence of waste heat generated by ICEs for EV cabin heating necessitates the consumption of energy from batteries, further reducing driving range. The positive temperature coefficient (PTC) heater is universally used in commercial EVs, but its low coefficient of performance (COP) of 0.9 to 0.95 [2] results in a 50–60% loss of driving range [3,4]. Although heat pump is a relatively new option with higher COP, a reversible vapour

compression heat pump system can still reduce a 10–15% driving range of EVs [5]. Additionally, the heating performance of traditional heat pump systems declines significantly with ambient temperature dropping [2]. For instance, when the ambient temperature dropped from 0 °C to -10 °C, the heating COP of an R134a heat pump system was reduced by 12.1%, and the cabin temperature fell from 23 °C to 11.5 °C [6]. Therefore, enhancing the battery capacity and cutting the electricity consumption of climate control devices [4] are the main approaches to extend the mileage without sacrificing passenger comfort. Using thermal energy storage (TES) devices offers a promising approach to provide cabin thermal management and improve driving distance of EVs. TES devices can be charged by external energy sources and supply heat to EVs without consuming onboard battery energy. This approach separates the heat source from batteries, allowing a greater proportion of battery power to be available for driving, thereby improving the driving range and overall performance of EVs.

The TES technologies, including sensible heat storage [7], latent heat storage [8], and thermochemical heat storage [9]–[13], have all been proposed as potential solutions for EV cabin climatization. Sensible or latent heat storage can offer relatively more steady heat charging/

* Corresponding author.

E-mail address: huashan.bao@durham.ac.uk (H. Bao).

Nomenclature			
A	cross-sectional area of the reactor (m^2)	amb	ambient
c_p	specific heat capacity ($J/(kg\ K)$)	cond	condenser
E_a	activation energy of adsorption (J/mol)	des	desorption
h	heat transfer coefficient (-)	evap	evaporator
k	pre-exponential factor of Arrhenius ($1/s$)	f	fluid
l	layer length (m)	f, in	inlet fluid
m	mass (kg)	f, out	outlet fluid
\dot{m}	mass flow rate (kg/s)	fw	between fluid and reactor
M	kinetic coefficient (-)	h	heating periods
p	overall heating power (kW)	n	number of the adsorption unit's layer
p'	heating power of a single adsorption unit (kW)	n,a	number of activated adsorption units
p_{ave}	average overall heating power (kW)	r	reactant
P	reactor pressure (Pa)	res	response
P_c	adsorption constraint pressure (Pa)	res, max	maximum allowable response
P_{eq}	equilibrium pressure (Pa)	rs	reactor stack
Q	heat (J)	sorb	sorbent
R	gas constant ($J/(mol\ K)$)	total	total condition of the system
t	time (s)	w	wall of reactor
T	temperature (K)	wr	between reactor wall and reactor
T_{eq}	equilibrium temperature (K)		
UA	overall heat exchange coefficient (W/K)	Abbreviation	
U_g	gravimetric energy density (kWh/kg)	AC	air conditioning
U_v	volumetric energy density (Wh/m^3)	Al-Si	aluminium silicon
V	volume (L)	COP	coefficient of performance
w	layer width (m)	ENG	expanded natural graphite
x	global conversion (-)	ENG-TSA	expanded natural graphite treated with sulfuric acid
		EVs	electric vehicles
		Exp	experiment
		HEVs	hybrid electric vehicles
		ICEs	internal combustion engines
		ICEVs	internal combustion engine vehicles
		MOF	metal-organic frameworks
		PCM	phase change material
		PTC	positive temperature coefficient
		SCP	specific cooling power
		Sim	simulation
		TES	thermal energy storage
Greek letters			
φ	mass ratio (-)		
ΔH_R	reaction enthalpy (J/mol)		
ΔS	reaction entropy ($J/(mol\ K)$)		
λ	thermal conductivity ($W/(m\ K)$)		
δ	thickness (m)		
Subscripts			
ads	adsorption		
air	air		

discharging over the time but lower energy density compared to thermochemical storage. In order to achieve reasonably compact storage unit, sensible or latent storage materials with high charging temperatures (over 500 °C) were proposed and studied for such application [7,8], which nevertheless requires rigorous heat preservation and insulation. It was found that a substantial heat loss (13–50%) of the total charged heat can occur during a 12-hour standstill period.

Thermochemical adsorption-based energy storage, which stores energy as chemical potential, provides higher energy density with minimal loss due to its temperature-independent storage mechanism. The adsorption reaction involves the interaction of a gaseous adsorbate with a solid adsorbent, accompanied by vast amounts of heat extraction for decomposition or desorption (energy charging) and heat release for synthesis or adsorption (energy discharging). The processes can be based on either thermophysical or thermochemical sorption [14]. Due to its advantage of being low grade heat-driven heat pumping/refrigeration process with high energy density and minimum loss during storage, adsorption cycles have been recognised as a promising alternative for automobile cabin climatization: adsorption heat pump cycles utilise the waste heat from engine exhaust gas or coolant water in internal combustion engine vehicles (ICEVs) to provide air conditioning (AC) [15]–[18]; adsorption thermal storage system provides cabin heating or cooling in EVs without consuming electricity from onboard batteries

[9]–[13].

Compared to thermophysical adsorption working pairs, such as the NaX zeolite – water pair [12], the zeolite SAPO-34 (AQSOA™ FAM-Z02, Mitsubishi Plastic Inc.) – water pair [13], and the CPO-27(Ni) metal-organic framework (MOF) – water pair [18] that have been studied for automobile cabin heating and cooling, thermochemical working pairs generally have larger heat storage capacities [19]. Additionally, compared to water adsorption, metal halide-ammonia thermochemical adsorption can operate and provide heating and cooling over a wider temperature range. In addition to air conditioning, metal halide-ammonia adsorption can be used for refrigeration in trucks [20] and is a superior option for heat pumping in cold regions, especially during winter when ambient temperature drops below 0 °C. Gardie et al. [11] studied the operation of a $MnCl_2-NH_3$ working pair sorption thermal storage system for EV cabin heating and cooling. For an ambient temperature of –10 °C, a sorption system that met the heating requirement of output fluid temperature of 35 °C and output power of 2 kW was studied. The specific energy density for heating was found to be 0.186 kWh/kg for reactive material and 0.090 kWh/kg for the whole system, and it had a system energy density of 92 kWh/m³.

Wang et al. [21] theoretically evaluated the equilibrium performance of different metal halide- NH_3 working pairs in sorption and resorption cycles for EV cabin heating and cooling, as they assumed the

sorption and resorption storage units were charged from the electrical grid when the EV battery was charged. They concluded that when the resorption high-temperature salt was the same as the sorption salt, the resorption cycle had a similar performance to the sorption cycle during wintertime but better performance during summertime. However, because resorption ACs require two adsorbent reactors, taking up more onboard space for installation, which makes them comparatively more suitable for e.g. passenger EVs. Jiang et al. [9] investigated adsorption heat storage using $\text{CaCl}_2\text{-NH}_3$ working pair and the composite adsorbent of CaCl_2 mixed with expanded natural graphite (ENG) matrix for EV cabin heating and cooling. To achieve the heating power requirement of 2.5 kW for 3 h in winter, it was found that the extra mass and volume for the sorption system required ranged from 72 kg and 0.060 m^3 to 44 kg and 0.033 m^3 at evaporation temperatures of $-15 \text{ }^\circ\text{C}$ and $10 \text{ }^\circ\text{C}$ respectively, which has limited influence on cruising mileage. This produced an energy density range of 125–227 kWh/m^3 (system-based) and a specific energy range of 0.104–0.170 kWh/kg (system-based). By assuming that 30% of battery electricity is consumed by conventional vapour compression heating, it was calculated that a maximum saved mileage of 100 km could be achieved by the proposed sorption AC system. An et al. [22] researched the optimal chemical working pairs for EV sorption AC in different temperature zones in China to work out the suitability of different working pairs for climate conditions. Focusing on energy density of the working pairs with varying temperatures, they concluded that MnCl_2 was the best for cold temperature zones and CaCl_2 was the best for warmer temperature zones. For a temperature zone requiring no cooling in summer and moderate heating in winter, a mix of CaCl_2 and MnCl_2 was found to be the optimum. This mix utilised the higher energy density of CaCl_2 at the higher evaporation temperatures and utilised the stable energy density of MnCl_2 at lower evaporation temperatures. The authors theoretically investigated the impact on the driving range, but only in summer conditions in a warm temperature zone, where it was found that CaCl_2 sorption AC extended the range of an EV by 9.4–37.7% compared with conventional AC. Zhang et al. [10] studied a two-adsorber beds resorption storage system based on $\text{CaCl}_2/\text{MnCl}_2\text{-NH}_3$ working pair for EV battery thermal management and cabin heating. The energy storage density was experimentally investigated as 0.097 kWh/kg (material-based), and the driving range in winter could be increased by 25.8% – 61.4% by implementing this combined cabin & battery thermal management strategy.

Previous studies have highlighted the potential of adsorption storage systems as a promising alternative of EV cabin climatisation for increasing driving range. Although sorption AC has a relatively larger volume and mass than conventional AC, studies have shown that the extra weight of the adsorption system has minimal impact on the vehicle's driving range and does not outweigh its benefits of consuming zero energy from the battery [9]. However, there remains a significant lack of research to gain practical insights. Previous studies have primarily focused on meeting energy requirements and selecting suitable working pair. Little attention has been given to the dynamic performance of such systems in terms of meeting power and response time requirements and stable heating or cooling output for EV cabin, and there is little effort on the optimisation of the adsorption reactor design to improve the power density and energy efficiency of the adsorption storage. Due to the nature of the thermochemical adsorption process, the discharge power delivered by the adsorption storage can vary significantly over time, providing an initial surge of power followed by attenuating power. To address this issue, modulating the adsorbate vapour transport [12] or varying the heat transfer fluid flow (air flow to deliver the heating/cooling power to the cabin) [11] was proposed and investigated for a steady performance with constant heating and cooling power and thermal potential. Although a simple flow control mechanism can effectively regulate the heating power and temperature, it was found that it would negatively impact the storage capacity, energy density, and therefore the overall efficiency of the system [23]. It is also critical to note that previous studies have only evaluated the performance of

sorption storage systems where a lumped mass of sorbent material interacts with adsorbate gas continuously over a long journey. However, for real-world driving scenarios with multiple short journeys, a considerable amount of energy would be lost to the sensible heating of the large reactor mass (including solid adsorbent materials and metallic components) as each time the vehicle starts a short journey with a few hours' intervals, because the entire reactor mass would need to be heated up from ambient temperature to the heat output temperature.

To address the abovementioned challenges and questions, this study introduces a novel modular reactor design for an adsorption thermal storage system for EV cabin heating in the UK climate. Instead of using a single sorption bed with a large volume bulk of sorbent, dividing it into multiple modular adsorption units enables a unique control strategy developed in this work, which controls the amount of adsorbent that interacts with the adsorbate gas rather than imposing constraints on the gas flow and working pressure. As a result, energy loss due to the sensible heating load of the entire reactor is minimised, as only the required amount of reactor mass is heated. Furthermore, individually controlled small modular units offer enhanced control over temperature and power output, enabling more stable thermal management of EV cabin. This work aims to thoroughly investigate the dynamic performance of the proposed adsorption heat storage reactor and demonstrate its efficient capability of providing stable and desirable heating output with zero consumption of EV onboard batteries, thereby providing insights into its real-world implementation.

2. Theory and method

2.1. Working principle

A simple adsorption system consists of two vessels, a solid–gas reactor containing solid adsorbent material and a condenser/evaporator for adsorbate gas, as shown in Fig. 1.

During the charge process, the reactor bed is heated (Q_{des}), leading to the desorption of the adsorbate gas from the solid adsorbent. The adsorbate gas is condensed in the connected condenser by the removal of condensation heat (Q_{cond}). The valve between the two vessels is then closed, enabling heat to be stored for long periods. The heat discharge process is initiated by opening the valve; the liquid adsorbate in the evaporator is evaporated by ambient heat (Q_{evap}), and is adsorbed by the solid adsorbent in the reactor. The two processes are driven by the pressure difference between the two vessels. The adsorption heat (Q_{ads}) is generated and exchanged with the heat transfer fluid for heating.

For the EV cabin heating application explored in this work, a fully charged adsorption storage system consists of adsorption reactor and evaporator. The desorption heat required for charging can be supplied by low-grade waste heat recovered from industrial plants or harnessing heat generated in solar farms. Depleted adsorption units or the entire adsorption reactor can be detached for recharging and replaced with a

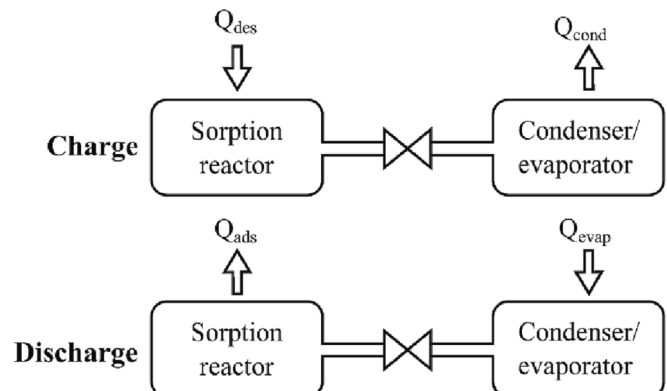


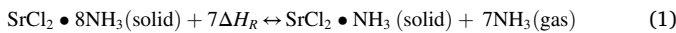
Fig. 1. Schematic of basic adsorption system configuration.

fully charged sorption reactor. Alternatively, the adsorption units can be directly electrically heated by using off-peak electricity from the municipal power grid, coinciding with the charging of EV batteries. While this option offers a more convenient charging solution, it may not be the most environmentally sustainable choice if the power grid is not completely decarbonised.

2.2. Adsorption material

Previously, MnCl_2 and CaCl_2 have been investigated as ammonia adsorption materials for electric vehicle cabin thermal management. However, recent studies have shown that $\text{SrCl}_2\cdot(8-1)\text{NH}_3$ is a promising working pair [24,25] for utilising and storing relatively lower temperature heat sources for spacing heating due to its relatively lower desorption temperature requirement compared to $\text{MnCl}_2\cdot(6-2)\text{NH}_3$ and higher specific energy storage capacity compared to both $\text{MnCl}_2\cdot(6-2)\text{NH}_3$ and $\text{CaCl}_2\cdot(8-4)\text{NH}_3$. Therefore, the designed system can be charged using low-grade heat below $100\text{ }^\circ\text{C}$ [26], such as solar thermal from flat plate solar collectors and industrial waste heat. The composite material of SrCl_2 in an ENG matrix with an adsorbent bulk density of 800 kg/m^3 and a mass ratio between SrCl_2 and ENG of 2:1 was used to improve the heat and mass transfer properties. The thermal conductivity of 2.4 W/(m K) was taken from a study by Jiang et al. [27].

The reversible reaction equation for the studied working pair of $\text{SrCl}_2\text{-NH}_3$ [28] is shown in Eq. (1):



This solid–gas thermochemical adsorption is mono-variant. The reaction equilibrium pressure can therefore be calculated from temperature using van't Hoff equation, Eq. (2):

$$\ln(P_{eq}) = -\frac{\Delta H_R}{RT} + \frac{\Delta S}{R} \quad (2)$$

where P_{eq} is equilibrium pressure (Pa), ΔH_R is reaction enthalpy (J/mol), R is gas constant (J/(mol K)), T is adsorbent temperature (K), and ΔS is reaction entropy (J/(mol K)).

Fig. 2 shows the P - T diagram of the reaction in equilibrium. In real-world applications, a temperature/pressure deviation from equilibrium condition must be created to drive the adsorption/desorption reaction. During energy charge, the desorbed ammonia is condensed by ambient heat at, for example, $25\text{ }^\circ\text{C}$, which gives a condensation pressure of about 10 bar and $\text{SrCl}_2\cdot(8-1)\text{NH}_3$ equilibrium temperature of $90\text{ }^\circ\text{C}$. However, the desorption temperature should be higher than $90\text{ }^\circ\text{C}$ to create a pressure difference between desorbed ammonia and condensation pressure. Similarly, during discharge, the discharge temperature should be lower than $73.5\text{ }^\circ\text{C}$ so that a pressure difference is created, driving the adsorption of evaporated ammonia at $5\text{ }^\circ\text{C}$.

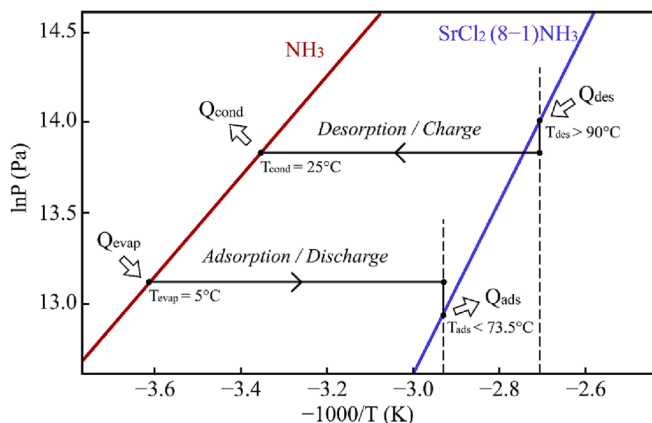


Fig. 2. P - T diagram of $\text{SrCl}_2\text{-NH}_3$ working pair.

2.3. Proposed adsorption system design

Fig. 3 shows the schematic of the proposed system modular design modelled in this work. The adsorption reactor stack consists of multiple modular adsorption units, each layer of which can be independently controlled by an individual valve to produce heat when required. These adsorption units can be utilised sequentially to avoid the consumption of substantial sensible heat at the onset of energy discharge and to achieve a rapid temperature increase of the supply air. The initiation of the adsorption reaction in each modular unit is controlled by opening the corresponding valve between that modular unit of the reactor and the evaporator. The implementation of such a valve control has been previously studied and demonstrated to enable precise control over the flow of working gas passing through selected layers of the unit [29].

To minimise the mass of extra components, such as heat exchangers, the air was chosen as the heat transfer fluid to be supplied directly to the cabin. The air to the reactor stack was selected to comprise a mix of 30% fresh air and 70% recirculated cabin air to improve thermal performance while providing adequate ventilation for passengers [30]. The relative humidity of the input air was set to the UK winter average of 88% [31] at all ambient temperatures considered.

3. Mathematical modelling and analysis

The dynamic performance of the proposed system was evaluated using a numerical simulation. The kinetic behaviour of the reaction and the heat transfer of the system were modelled with the following conditions.

- There is negligible heat transfer between modular adsorption units since there is no direct contact between units.
- The initial system temperature is equal to the ambient temperature.
- The inlet air temperature of the modular adsorption unit is equal to the outlet air temperature of the previous unit in the stack, neglecting the heat loss of the air due to the very short flowing distance between two units.
- Air is only directed through activated modular adsorption units such that the supply air entering the vehicle cabin is the outlet air from the most recently activated layer, which can be achieved by using an effective valve-controlled system as reported in work [29].
- The evaporator side was modelled at constant pressure for all layers throughout the adsorption process, considering the evaporator temperature can be maintained at a constant value.
- There is no pressure drop between evaporator and reactor [32].

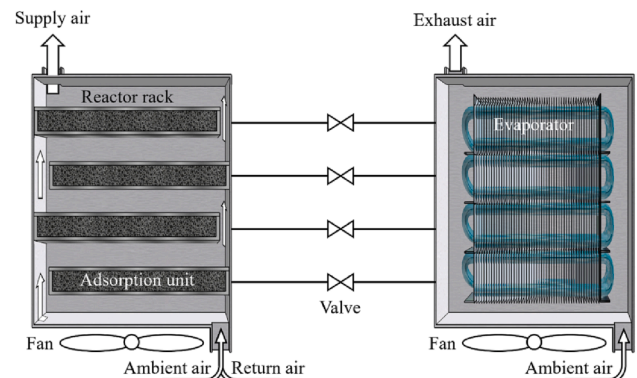


Fig. 3. Schematic diagram of the proposed modular adsorption system during energy discharging process.

3.1. Kinetic model

The adsorption reaction is driven by the pressure difference between equilibrium conditions and reactor conditions. At the beginning of the adsorption reaction, reaction rate is high due to large pressure differences, but it slows down as equilibrium is approached [33]. A kinetic model developed by Huang et al. [34] for $\text{SrCl}_2 \cdot (8-1)\text{NH}_3$ adsorption was used in this work, as given in Eq. (3)

$$\frac{dx}{dt} = k_o \exp\left(\frac{-E_a}{RT}\right) (1-x)^M \left(\frac{P_c - P_{eq}}{P_{eq}}\right) \quad (3)$$

where x is the global conversion of the adsorption process, a value between 0 and 1, representing the ratio of the mass of adsorbate that is actually adsorbed by the sorbent to the maximum mass of adsorbate that can be adsorbed; T is the adsorbent temperature, P_c is the adsorption constraint pressure which is the evaporation pressure of ammonia in the evaporator. The values of the coefficients used were $k_o = 0.019$, $E_a = 6921$, and $M = 2.96$. The thermodynamic equilibrium pressure P_{eq} was calculated Eq. (2).

3.2. Heat transfer model

The modular adsorption unit was modelled, and the heat transfer process is schematically shown in Fig. 4. Eqs (4), (5), and (6) are the used energy balance equations among air, reactor wall, and reactant (adsorbent material).

For the heat transfer fluid:

$$m_f c_{p,f} \frac{dT_f}{dt} = \dot{m}_f c_{p,f} (T_{f,in} - T_{f,out}) - (UA)_{fw} (T_f - T_w) \quad (4)$$

$$(UA)_{fw} = \frac{A}{\frac{1}{h_f} + \frac{\delta_w}{\lambda_w}} \quad (5)$$

where m_f is the mass of heat transfer fluid, \dot{m}_f is the mass flow rate of heat transfer fluid, $c_{p,f}$ is the specific heat capacity of the fluid, T_f is the fluid temperature, $T_{f,in}$ is the inlet fluid temperature, $T_{f,out}$ is the outlet fluid temperature, $(UA)_{fw}$ is the overall heat exchange coefficient between heat transfer fluid and reactor wall, T_w is reactor wall temperature, h_f is the heat transfer coefficient of air, A is the cross-sectional area of the reactor, δ_w and λ_w are the thickness and thermal conductivity of the reactor wall, respectively.

For the reactor wall:

$$m_w c_{p,w} \frac{dT_w}{dt} = (UA)_{fw} (T_f - T_w) - (UA)_{wr} (T_w - T_r) \quad (6)$$

$$(UA)_{wr} = \frac{A}{\frac{\delta_r}{\lambda_r} + \frac{\delta_w}{\lambda_w}} \quad (7)$$

where $(UA)_{wr}$ is the overall heat exchange coefficient between the reactor wall and the reactant, T_r is the reactant temperature, δ_r and λ_r are the thickness and thermal conductivity of the reactant, respectively.

For the reactant:

$$m_r c_{p,r} \frac{dT_r}{dt} = (UA)_{wr} (T_w - T_r) + n_{\text{NH}_3} \Delta H_R \frac{dx}{dt} \quad (8)$$

where n_{NH_3} is the total mole number of adsorbed ammonia gas.

The lumped heat capacity of reactants includes the heat capacity of ENG, SrCl_2 , and transient amount of adsorbed NH_3 , as shown in Eq. (9):

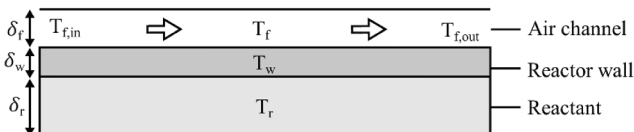


Fig. 4. Heat transfer schematics of air and reactant.

$$m_r c_{p,r} = m_{\text{ENG}} c_{p,\text{ENG}} + m_{\text{SrCl}_2} c_{p,\text{SrCl}_2}(T_r) + x m_{\text{NH}_3} c_{p,\text{NH}_3} \quad (9)$$

where m_{NH_3} is the total mass of adsorbed ammonia gas.

The temperature of the air was calculated to be the average of the inlet and outlet temperature, as shown in Eq. (10):

$$T_f = \frac{T_{f,in} + T_{f,out}}{2} \quad (10)$$

The heating power of a single adsorption unit n can be calculated as Eq. (11):

$$\dot{p}_n = \dot{m}_f c_{p,f} (T_{fn,in} - T_{fn,out}) \quad (11)$$

where $T_{fn,in}$ and $T_{fn,out}$ is the inlet and outlet temperature of unit n .

For the first adsorption unit,

$$\dot{p}_1 = \dot{m}_f c_{p,f} (T_{f1,in} - T_{f1,out}) \quad (12)$$

When n greater than 1, because $T_{fn,in}$ is assumed to be equal to the outlet air temperature of the previous unit $T_{f(n-1),out}$, the Eq. (11) can be expressed as Eq. (13):

$$\dot{p}_n = \dot{m}_f c_{p,f} (T_{f(n-1),out} - T_{fn,out}) \quad (13)$$

The heating power of n units is a cumulative value from unit 1 to unit n , shown as Eq. (14):

$$p_n = \dot{p}_1 + \dot{p}_2 + \dots + \dot{p}_n \quad (14)$$

The average overall heating power can be calculated by Eq. (15):

$$p_{ave} = \frac{\int p_{n,a} dt}{t_{total}} \quad (15)$$

where $p_{n,a}$ is the cumulative heating power of the activated adsorption units, and t_{total} is the total operating time of the system.

3.3. System design parameters and performance analysis

The heating system used in vehicles is to keep the cabin air temperature between 21 and 25 °C, and should have a heating response time (time taken to reach the minimum required supply air temperature) of 2 min. The heating power requirement for vehicle cabin heating varies depending on ambient temperatures, as presented in Table 1.

To achieve the abovementioned heating requirement, the adsorption heat storage system was designed with the parameters given in Table 2. A layer with a width of 0.15 m and a length of 0.25 m was used. The mass of SrCl_2 in each layer was 0.34 kg, corresponding to the mass required for reaction with 15 mol of ammonia.

Fig. 5 illustrates the performance analysis framework for the proposed system. The investigation focused on the system's dynamic performance in terms of the supply air temperature, heating power output, global conversion, and energy density of the adsorption storage system. This work explored the system's performance at ambient temperatures ranging from -5 to 10 °C and conducted sensitivity analyses on design dimensions to assess their impact on system performance.

3.4. System control

A control strategy was used to determine when and which modular adsorption unit should be activated for ammonia adsorption. To ensure that the air temperature reaches 21 °C within the required response time, it is necessary to activate multiple modular units simultaneously at the start of the heating period. Because the system recirculates air, it is

Table 1
Steady-state output power requirements [35].

Ambient temperature, T_{amb} (°C)	-5	0	5	10
Heating power (kW)	2.4	1.7	1.3	0.8

Table 2
Design parameters of adsorption heat storage reactor for EV cabin heating.

Parameter	Value
Air temperature range, $T_{f,out}$ (°C)	21–25
Maximum allowable response time ^a , $t_{res,max}$ (s)	120
Heat transfer fluid channel thickness, δ_f (m)	0.02
Wall thickness, δ_w (m)	0.002
Modular unit width, w (m)	0.15
Modular unit length, l (m)	0.25
Mass of SrCl ₂ per modular unit ^b , m_{SrCl_2} (kg)	0.34
Mass ratio of salt to ENG, ϕ_r (-)	2:1
Specific heat capacity of ENG, $c_{p,ENG}$ (kJ/(kg K))	0.61
Bulk density of reactant, ρ_r (kg/m ³)	800
Thermal conductivity reactant, λ_r (W/(m K))	2.4
Density of wall ^c , ρ_w (kg/m ³)	8000
Thermal conductivity of wall ^c , λ_w (W/(m K))	15
Specific heat capacity of wall ^c , $c_{p,w}$ (kJ/(kg K))	0.468
Reaction enthalpy, ΔH_R (J/mol)	41,431
Reaction entropy, ΔS (J/mol/K)	228.8
Mass ratio of fresh air to recirculated air, ϕ_{air} (-)	3:7

^a Time required to reach a minimum output temperature of 21 °C.
^b Required mass of SrCl₂ for adsorption of 15 mol of ammonia per layer.
^c Wall material used was stainless steel-316.

challenging to determine the initial number of units required to achieve the desired temperature. Therefore, a trial-and-error approach was employed. After the initial units were activated, the next unit was activated when the outlet air temperature fell below 21 °C.

A second control strategy was also proposed and examined. Instead of a predetermined initial number of modular adsorption units, the supply air temperature was monitored and checked at regular intervals (15 s / 50 s / 100 s). When this temperature fell below 21 °C, an additional adsorption unit was activated.

4. Results and discussion

The adsorption storage system was studied at an ambient temperature range of - 5–10 °C for heating periods of 1 and 2 h. The supply air temperature, heating power, global conversion of adsorption and energy storage density were obtained and analysed. The impact of surface area of modular adsorption unit (0.040–0.123 m²) and SrCl₂ mass (0.113–0.555 kg) in each unit on the system performance was also investigated by modelling the system for a heating period of 1000 s.

4.1. Supply air temperature

According to the predetermined layer control strategy, 6 adsorption units were activated simultaneously at the beginning of the heating

period at the ambient temperature of 5 °C. It reached the target temperature of 21 °C by 64.5 s, as shown in Fig. 6. On the other hand, if the second control strategy was used, only the sampling time of 15 s could satisfy the requirement of heating response time of 120 s, which took 115 s to heat the air to more than 21 °C. However, it produced an overshoot temperature of 26.9 °C, exceeding the acceptable temperature range of 21–25 °C. This indicated that the short sampling time interval overestimated the number of adsorption units required. Comparatively, sampling times of 50 s and 100 s did not lead to temperature overshoot, the maximum supply air temperature reached was within the acceptable temperature range, however, the response time is longer than 120 s for the supply air to reach 21 °C.

For all control strategies, a total of 7 modular adsorption units were activated by 800 s, indicating that the control strategy has little impact on the total number of unit used over the entire heating period but only affect the response time of the heating system. It was then decided that the system should use a predetermined number of adsorption units activated simultaneously (first control strategy) to provide quick heating for vehicle cabin.

When 6 adsorption units were activated simultaneously at the beginning of heating, the initial outlet fluid temperature increased from an ambient temperature of 5 °C to a peak temperature of 22.4 °C. The maximum temperature of the reactor was 68.4 °C, and the maximum temperature of the reactor wall was 49.2 °C. After the initial temperature increase, it was found that one more adsorption unit had to be

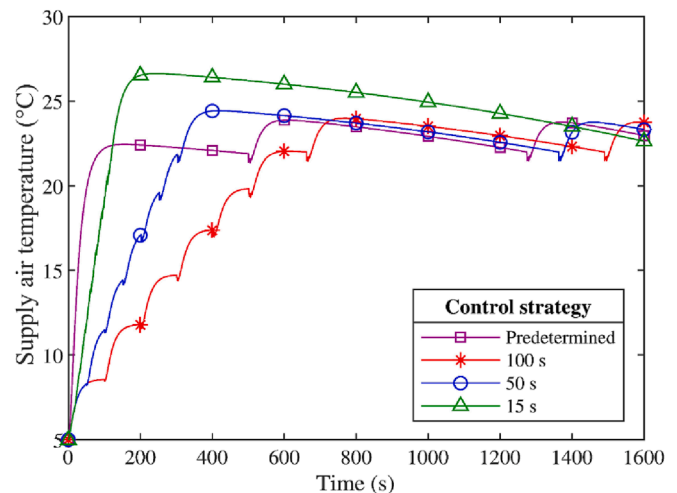


Fig. 6. Supply air temperature for different control strategies, $T_{amb} = 5$ °C.

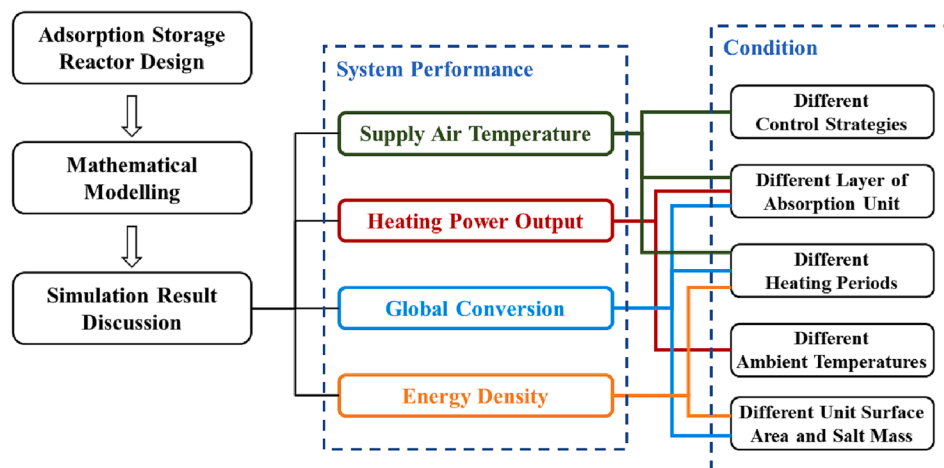


Fig. 5. The framework of performance analysis of the proposed adsorption storage system.

activated approximately every 534 s to sustain a temperature output within the required range. For a heating period of 1 h, 12 adsorption units in total were required to maintain a heating power of 1.3 kW and supply air temperature between 21 and 25 °C, as shown in Fig. 7. The air mass flow rate was 0.242 kg/s. The supply air to the cabin had a peak temperature of 23.9 °C.

As the supply air to the cabin was taken from the latest activated adsorption unit, a slight temperature drop of 0.5 °C occurred whenever a new unit was activated. This drop could be avoided by taking the air from the previous adsorption unit until the temperature of the new unit exceeds the previous unit. However, this would require extra temperature sensors and a more complex control strategy. As the heat released from the adsorption reaction declined with time, the air temperature at the outlet of each activated unit decreased, but a temperature jump was achieved whenever a new unit was activated because of the usage of recirculated air, as can be seen in Fig. 7.

4.2. Heating power

Fig. 8 presents the heating power in the energy discharge process of the adsorption storage, including the overall heating power and heating power of the selected adsorption units, for a heating period of 1 h at the ambient temperature of 5 °C. The average overall heating power achieved is 1.3 kW. As a new unit was activated, there was a drop in overall heating power caused by the low initial power output of the newly activated adsorption reaction and the energy consumption by the initial sensible heating load of the adsorption unit. The heating power of each individual adsorption unit behaved similarly to the power profile of Unit 1, having a peak power output of 0.20–0.22 kW. In the figure, the heating powers of Units 4, 7, and 10 are cumulative values, including the sum of the power output from previously activated units.

The output temperature and power fluctuations is less than 0.5 °C and 0.22 kW, respectively, indicating a high level of heating supply stability. This stability surpasses that of previous works [10,12,13], which encountered output temperature and power fluctuations exceeding 10 °C and 0.5 kW, respectively.

The required heating power changed with the ambient temperatures. Table 3 displays the required system sizes and output parameters at an ambient temperature range of –5–10 °C for a heating time of 1 h. The airflow rate and number of modular units of the adsorption system were adjusted for each ambient temperature to achieve the requirement of output temperature and power.

Fig. 9 exhibits the system heating power at different ambient temperatures. The results demonstrated that the required heating power could be achieved at the entire ambient temperature range of –5–10 °C.

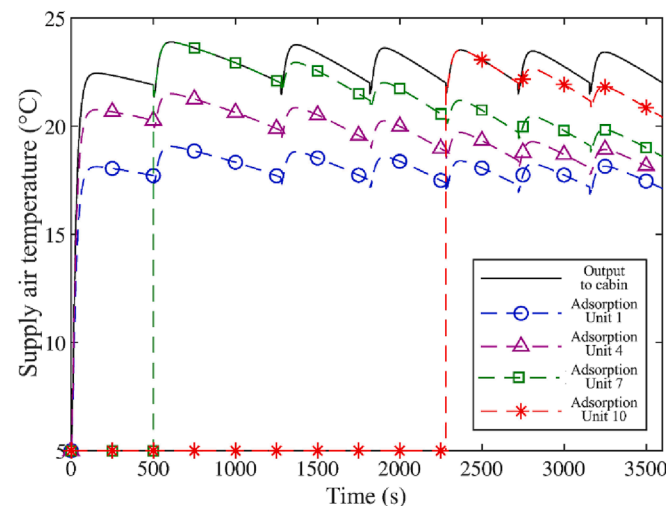


Fig. 7. Air temperature using the first control strategy, $T_{amb} = 5\text{ }^{\circ}\text{C}$.

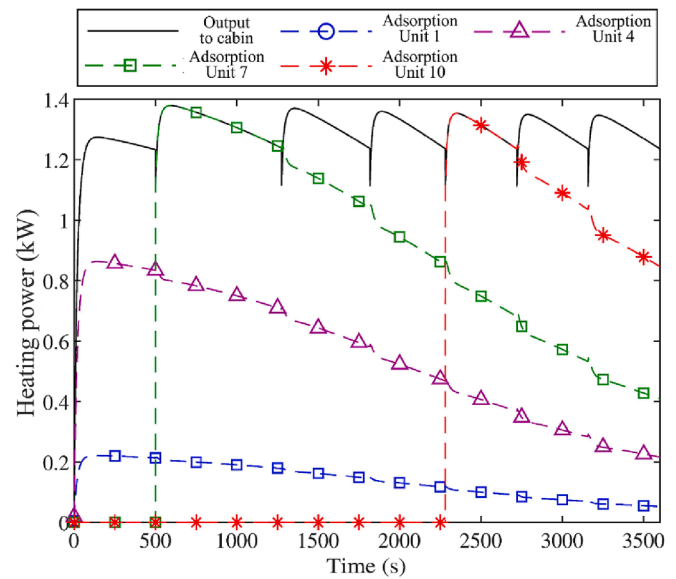


Fig. 8. Heating power of the adsorption storage system, $T_{amb} = 5\text{ }^{\circ}\text{C}$.

Table 3

System requirements and performance for different ambient temperatures.

Ambient temperature (°C)	-5	0	5	10
Heating power requirement (kW)	2.4	1.7	1.3	0.8
Total modular unit number (-)	23	16	12	7
Air flow rate (kg/s)	0.290	0.249	0.242	0.202
Response time (s)	76	65.5	64.5	44

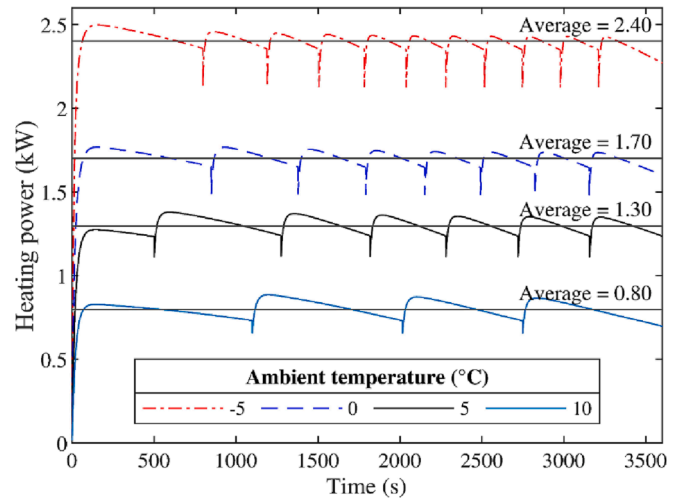


Fig. 9. System heating power at different ambient temperatures.

The response time was longer at lower ambient temperatures due to the increased sensible heat load but remained well below the necessary response time of 120 s. At lower ambient temperatures, as shown in the figure, the frequency of activating a new adsorption unit was higher to maintain the temperature of the supply air within the required range.

4.3. Global conversion and system energy density

Global conversion is defined as the ratio of the adsorbent reacted with ammonia to the total adsorbent in the adsorption units [36]. Fig. 10 shows the evolution of global conversion of the whole system as well as selected individual adsorption units. The initially activated units have a

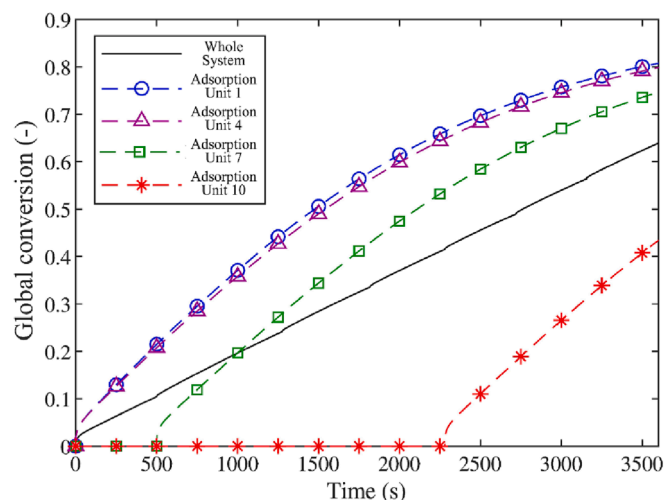


Fig. 10. Global conversion profile, $T_{amb} = 5\text{ }^{\circ}\text{C}$.

high global conversion at the end of the heating period of 0.8, as exemplified by Unit 1 and Unit 4 in the figure. However, Unit 10, activated at 2280 s, only reached a global conversion of 0.43 at the end of the heating period of 1 h. The global conversion of the whole system reached 0.64 at the end of the heating period.

Although the adsorbent material exhibited a gravimetric energy density of 211.8 Wh/kg, the overall energy density of the adsorption storage reactor was reduced to 79.2 Wh/kg when the mass of the metallic components of the reactor was taken into account. Table 4 provides an overview of various TES systems that have been studied for automotive cabin climatization, including some results from this work. Comparing this system's material energy density to TES systems previously studied (as shown in Table 4), it is 1.6 times higher than the NaX Zeolite-Water system [12] and nearly comparable to other sorption systems that use SAPO-34-Water [13] or $\text{CaCl}_2\text{-NH}_3$ [9] as working pairs. However, when considering the volume of the container and airflow channel, the volumetric energy density of this multi-modular system decreased from 169.4 kWh/m³ for the material only to 73.8 kWh/m³, which is 2.7 times lower than that of a single-bed sorption system [9]. These findings emphasise the importance of accounting for the volume and mass of the entire stack when reporting energy density and highlight the trade-off between volumetric energy density and stable heating supply in the multi-module design.

As the ambient temperature increases from $-5\text{ }^{\circ}\text{C}$ to $10\text{ }^{\circ}\text{C}$, the gravimetric and volumetric energy density of the adsorption system both improved by about 9.4% due to the reduced sensible heating load, and the global conversion at the end of the heating time grew by 7.2% from 0.62 to 0.67. This is a notable result as the system has a relatively stable energy efficiency over the ambient temperatures of $-5\text{--}10\text{ }^{\circ}\text{C}$. Compared to this, vapour compression heat pumps suffer a dramatic reduction in heating capacity and COP at low ambient temperatures.

When expanding the heating periods from 1 h to 2 h at an ambient temperature of $5\text{ }^{\circ}\text{C}$, the total required heating capacity was doubled to 2.6 kWh, however, the adsorption unit number only increased by 66.7% to 20 layers. This was a result of the higher global conversion of the initially reacted layers by the end of 2 h heating period. The global conversion for a heating period of 2 h was 21.7% higher than for a heating time of 1 h, leading to a 20.0% and 19.3% increase in gravimetric energy density and volumetric energy density, respectively. For journeys shorter than 1 h, the final global conversion will be even lower than 0.64, making it essential that the valves can be closed at the end of the heating period to prevent energy loss. These partially reacted units could then be used for the next heating cycle or fully recharged.

These results indicate that the final global conversion was lower than the values obtained in other studies focused only on meeting energy

demand requirements. Modelling dynamics process of adsorption is then crucial since not all expected adsorption reactions can be proceeded within a given heating time. Thus the needed scale of adsorption system is larger than the calculated value by only considering energy storage capacity of adsorption system.

4.4. Impact of size of adsorption unit

The impact of surface area of adsorption unit (heat transfer surface) and mass of SrCl_2 in each unit on the adsorption system performance were investigated by modelling a system with 7 units and an airflow rate of 0.242 kg/s at the ambient temperature of $5\text{ }^{\circ}\text{C}$. In this analysis, the mass of SrCl_2 per unit ranged between 0.113 and 0.555 kg. Because of the used constant adsorption material density and mass ratio of SrCl_2 to ENG, the volume of adsorbent material was the same at the same salt mass. The heat transfer surface area of the unit varied from 0.04 m^2 to 0.1225 m^2 , as presented in Table 5. The ratio between unit length and width for this analysis was kept constant at 1:1. Due to the constant value of airflow channel height, a larger unit surface area leads to a larger air channel volume.

Fig. 11 shows the impact of adsorption unit dimensions on the volumetric power density of adsorption system over a period of 1000 s. The volumetric power density of adsorption system is directly proportional to heat transfer capacity and inversely proportional to system volume. Hence there is a dilemma in designing unit area since a larger heat transfer surface area can amplify heat transfer while also expanding the overall system volume. The results in Fig. 11 indicated that a small surface area would be favourable as the reduced total volume outweighed any benefits of increased heat transfer. At the same SrCl_2 mass of 0.18 kg, an area enlarged from 0.04 m^2 to 0.0625 m^2 decreased the power density by 24% (from 143.3 kW/m^3 to 115.7 kW/m^3). On the other hand, with higher SrCl_2 mass, the advantage of smaller unit areas in high power density was fading away. This is because a smaller surface area will add more thickness under the same mass addition of SrCl_2 and get more adverse effects of heat transfer reduction. Hence, the power density of smaller layer areas was more sensitive to changes in the thickness of SrCl_2 per adsorption unit.

For each surface area, there was an optimum mass of SrCl_2 per unit at which the enhanced heat transfer from less SrCl_2 thickness and larger air channel was balanced with higher energy output from the adsorption reaction. The peak power density of the adsorption unit from the dimensions tested was 143.3 kW/m^3 with a unit area of 0.04 m^2 and 0.18 kg of SrCl_2 per unit. The optimum power density was higher than that of the design in Table 2 because the average power output was limited to 1.3 kW, resulting in a low power density of 74.3 kW/m^3 . However, these results show that higher power densities are possible if higher heating power is required. The power output could be further increased by increasing the mass flow rate of air. The energy density of the system with varying dimensions followed a similar trend to power density, with a smaller layer area having better performance at a lower mass of SrCl_2 per unit.

Fig. 12 shows the global conversion of the adsorption system after 1000 s with varying unit surface areas and mass of SrCl_2 per unit. With given surface area, less SrCl_2 inside each adsorption unit means thinner adsorbent layer, the final global conversion is higher because there is less stored energy which discharges relatively quicker with better heat transfer. Under the same mass of SrCl_2 per unit, with a larger surface area and better heat transfer between adsorbent and air, a lower adsorption temperature and pressure are needed, therefore, the adsorption reaction is quicker according to the kinetic equation, Eq. (3), leading to a higher global conversion rate. In this case, for example, when using 0.18 kg SrCl_2 per adsorption unit, even though using 0.1225 m^2 surface area leads to a higher final global conversion (0.71) compared to that of using 0.04 m^2 surface area (0.56), the overall system volume is too large causing a lower power (energy) density as can be seen in Fig. 11.

Table 4
Overview of TES systems studied for vehicle cabin climatisation.

TES Type	Application	Ref.	Storage Material	Required Charge Temperature	Discharge Output Temperature		Ambient	Discharge Time	Heating/ Cooling Capacity	Mass		Volume	Energy Density		COP	Study Type				
				°C	Mode	°C				°C	Hours		kWh	kg			Beds	L	Wh/kg	kWh/m ³
Solid Media	EVs	[7]	Nickel-Chromium Alloy	850	Heating	60	−10	0.5	2.5	22.5	-	-	-	-	-	Exp				
PCM		[8]	Silicon Carbide	725						13.8			142.5 ^b	187.3 ^b						
			Aluminium-Silicon Alloy	600	Heating	56–57	−10	3.95–4.4	5.8–6.1	18.8	32	40.2	225 ^b	179 ^b	–	Exp				
Adsorption		[9]	CaCl ₂ -NH ₃ within ENG matrix	120	Heating	25 ^a	10	3	7.5	–	44	33	170 ^b	197 ^b	0.82	Sim				
		[10]	CaCl ₂ -NH ₃ and MnCl ₂ -NH ₃ within ENG-TSA matrix	165	Heating	40 ^a	–	1	1.7	6	–	5.69	104 ^b	125 ^b	0.34	Exp				
		[11]	MnCl ₂ -NH ₃ within ENG matrix	100	Heating	35 ^a	−10	2	4	3.5	–	–	186 ^b	92 ^b	–	Sim				
		[12]	NaX Zeolite - Water	300	Cooling	15 ^a	40	1	0.9	5	20	11.86	93 ^b	45 ^b	–	Exp & Sim				
		<i>This Study</i>	SrCl ₂ -NH ₃ within ENG matrix	90	Heating	21–25	5	1	1.3	6	16.4	17.5	130 ^d	85 ^e	–	Exp & Sim				
								2	2.6	10	27.3	29.2	95 ^d	60 ^a	0.64 ^g	Sim				
	HEVs	[13]	SAPO-34 - Water	95	Heating	40 ^a	10	0.5	0.68	3.3	9	15.3	211.8 ^c	73.8 ^b	0.78 ^g	Exp & Sim				
					Cooling	20 ^a	35	0.5	0.55				254.1 ^c	88.6 ^b		Sim				
	ICEVs	[15]	Mixture of CaCl ₂ and MnCl ₂ - NH ₃ within ENG-TSA matrix	210–240	Cooling	–	30	0.5	4	–	240	316.5	215.6 ^c	177.5 ^c	–	Exp & Sim				
		[16]	CaCl ₂ -NH ₃ and MnCl ₂ - NH ₃ within ENG matrix	157.2–128.4	Cooling	−10	30	45	1.8	–	80	–	–	–	–	Exp				
						−20		1	1.9						1.4	Sim				
		[17]	Silica Gel - Water	90	Cooling	–	28	0.56	0.51	2	86 ^f	–	–	–	0.34	Exp & Sim				
		[18]	CPO-27(Ni) - Water	130	Cooling	12 ^a	30	0.25	2.4	5.4	–	–	440 ^b	–	0.47	Exp & Sim				

^a Designed output temperature, not the actual output temperature from experiments or simulations.

^b Energy density of the total thermal storage tank or sorption bed, including thermal storage materials and its container.

^c Energy density of sorbent.

^d Powers density (W/kg) of total materials, including sorbent and vapour.

^e Power density (W/kg or kW/m³) of sorbent.

^f Mass of the total system.

^g Final global conversion of adsorption reaction. [7891011121315161718].

Table 5
Unit surface area and air channel volume.

Unit length (m)	Unit width (m)	Unit surface area (m ²)	Airflow channel volume (L)
0.20	0.20	0.0400	0.80
0.25	0.25	0.0625	1.25
0.30	0.30	0.0900	1.80
0.35	0.35	0.1225	2.45

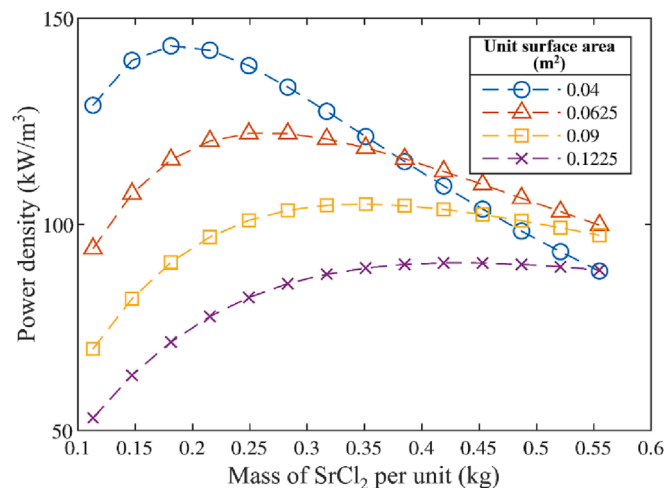


Fig. 11. Average power density of adsorption system over first 1000 s at different unit surface area and salt mass, $T_{amb} = 5\text{ }^{\circ}\text{C}$.

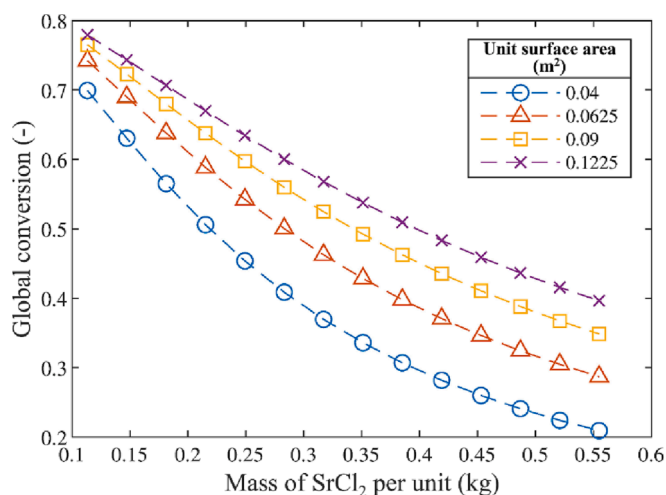


Fig. 12. Global conversion of adsorption system with different surface area of adsorption unit after 1000 s, $T_{amb} = 5\text{ }^{\circ}\text{C}$.

5. Recommendations for further work

The potential of a modular designed thermochemical adsorption heat storage system to meet temperature, power, and response time requirements for EV cabin heating has been explored. This work focused on the modular reactor design and the dynamic adsorption performance. For a more comprehensive analysis of system performance, it is necessary to consider the volume and mass of evaporator, valves, and fan. Further work should aim to optimise design dimensions not covered in this study, such as ratio of layer width and length, wall thickness, and air channel.

The feasibility of a practical realisable, cost-effective design for the modular reactor with independently controlled adsorption units, as

described in this work, requires further exploration. The control strategy of the system can be further refined by adjusting the mass flow rate of air to achieve the desired output temperature and heating power. Additionally, the recirculation ratio of air may significantly impact system performance and warrants further investigation.

The proposed design offers a solid foundation for improving cycle performance. While battery waste heat is insufficient to fulfil cabin thermal management requirements independently, additional research could explore integrating battery thermal management with the cabin heating system, potentially improving both cabin heating performance and battery performance. For example, battery waste heat could be used as evaporation heat input, resulting in higher heating power and increased energy density for the adsorption cycle. Furthermore, this study does not address evaporator defrosting, so the potential utilisation of waste battery heat or a small percentage of adsorption heat to defrost the evaporator deserves further examination.

6. Conclusion

This work studied the potential of using thermochemical adsorption heat storage for EV cabin heating, providing an alternative to current state-of-the-art technology. The proposed system consumes minimal battery electricity and can be charged using low-grade renewable heat and/or industrial waste heat.

The adsorption system was studied for heating periods of 1 and 2 h at the ambient temperature range of $-5\text{--}10\text{ }^{\circ}\text{C}$ to reflect the practical system performance at the typical operating conditions of a vehicle. By focusing on adsorption kinetics in this work, the major conclusions are:

- For an adsorption system with 12 modular adsorption units, an average heating power of 1.3 kW and supply air temperature range of $22\text{--}23.9\text{ }^{\circ}\text{C}$ with a response time of 64.5 s can be achieved for the heating periods of 1 h at an ambient temperature of $5\text{ }^{\circ}\text{C}$.
- The efficiency of the adsorption system was stable with varying ambient temperatures, with an increase of final global conversion from 0.62 to 0.67 as the ambient temperature varied from $-5\text{--}10\text{ }^{\circ}\text{C}$.
- Modelling adsorption dynamics is crucial since not all expected adsorption reactions can proceed within a given heating time. The power density of an adsorption unit can theoretically reach 143.3 kW/m^3 , while 74.3 kW/m^3 is enough for the system to achieve the required heating power of 1.3 kW. Hence, higher heating power is possible if required.
- The power and energy densities of the system have similar varying trends as varying dimensions of adsorption unit, with a smaller unit heat transfer surface area and lower mass of SrCl_2 per unit having better performance. The response time and energy density for a smaller unit area were more sensitive to changes in the mass of SrCl_2 per unit.

CRedit authorship contribution statement

Megan Wilks: Writing – original draft, Methodology, Data curation, Software, Investigation. **Chenjue Wang:** Validation, Writing – review & editing, Visualization. **Janie Ling-Chin:** Writing – review & editing. **Xiaolin Wang:** Writing – review & editing. **Huashan Bao:** Supervision, Resources, Conceptualization, Methodology, Writing – review & editing, Visualization, Project administration.

Declaration of Competing Interest

The authors declare that they have no known competing financial interests or personal relationships that could have appeared to influence the work reported in this paper.

Data availability

Data will be made available on request.

Acknowledgement

The authors gratefully acknowledge the support from the Solar S&HP project (EP/T023090/1), the H + C Zero Network (EP/T022906/1), the GEMS project (EP/V042564/1) and Durham University EPSRC IAA (EP/R511523/1) funded by the Engineering and Physical Science Research Council of the UK.

References

- Government takes historic step towards net-zero with end of sale of new petrol and diesel cars by 2030 - GOV.UK, 2020. <https://www.gov.uk/government/news/government-takes-historic-step-towards-net-zero-with-end-of-sale-of-new-petrol-and-diesel-cars-by-2030> (accessed Jul. 25, 2022).
- Lee H, Lee D, Kim Y. Heating performance of a coolant-source heat pump using waste heat from stack and electric devices in fuel cell electric vehicles under cold conditions. *Energy Convers Manag* Jan. 2022;252:115092. <https://doi.org/10.1016/J.ENCONMAN.2021.115092>.
- Li W, Liu R, Liu Y, Wang D, Shi J, Chen J. Performance evaluation of R1234yf heat pump system for an electric vehicle in cold climate. *Int J Refrig Jul*. 2020;115: 117–25. <https://doi.org/10.1016/J.IJREFRIG.2020.02.021>.
- Zhang Z, Wang D, Zhang C, Chen J. Electric vehicle range extension strategies based on improved AC system in cold climate – A review. *Int J Refrig Apr*. 2018;88: 141–50. <https://doi.org/10.1016/J.IJREFRIG.2017.12.018>.
- Zhang Z, Wang J, Feng X, Chang L, Chen Y, Wang X. The solutions to electric vehicle air conditioning systems: A review. *Renew Sustain Energy Rev Aug*. 2018; 91:443–63. <https://doi.org/10.1016/J.RSER.2018.04.005>.
- Wang Z, Wei M, Peng F, Liu H, Guo C, Tian G. Experimental evaluation of an integrated electric vehicle AC/HP system operating with R134a and R407C. *Appl Therm Eng May* 2016;100:1179–88. <https://doi.org/10.1016/J.APPLTHERMALENG.2016.02.064>.
- Dreibigacker V, Belik S. High temperature solid media thermal energy storage system with high effective storage densities for flexible heat supply in electric vehicles. *Appl Therm Eng Feb*. 2019;149:173–9. <https://doi.org/10.1016/J.APPLTHERMALENG.2018.12.026>.
- Luo C, et al. Prototype design and experimental study of a metal alloy-based thermal energy storage system for heat supply in electric vehicles. *J Energy Storage Jul*. 2022;51:104393. <https://doi.org/10.1016/J.EST.2022.104393>.
- an L, Wang RZ, Li JB, Wang LW, Roskilly AP. Performance analysis on a novel sorption air conditioner for electric vehicles. *Energy Convers Manag* 2018;156: 515–24. <https://doi.org/10.1016/J.ENCONMAN.2017.11.077>.
- Zhang C, Wu S, An G, Wang L. Resorption thermal energy storage strategy based on CaCl₂/MnCl₂-NH₃ working pair for battery electric vehicles. *Chem Eng J Aug*. 2022;441:136111. <https://doi.org/10.1016/J.CEJ.2022.136111>.
- Gardie P, Goetz V. Thermal Energy Storage System by Solid Absorption for Electric Automobile Heating and Air-Conditioning. *SAE Technical Papers Feb*. 1995. <https://doi.org/10.4271/950017>.
- Narayanan S, et al. A thermophysical battery for storage-based climate control. *Appl Energy Mar*. 2017;189:31–43. <https://doi.org/10.1016/J.APENERGY.2016.12.003>.
- Engel G, et al. Development of a sorption thermal energy storage to support the thermal management of hybrid vehicles. *Int J Veh Des* 2021;85(2–4):139–53. <https://doi.org/10.1504/IJVD.2021.120411>.
- H. Bao and Z. Ma, Thermochemical energy storage, *Storing Energy: with Special Reference to Renewable Energy Sources*, pp. 651–683, 2022, doi: 10.1016/B978-0-12-824510-1.00028-3.
- Gao J, Wang LW, Tian YC. Numerical and experimental investigation of multi-halide chemisorption system for exhaust gas heat recycling. *Appl Therm Eng Jul*. 2021;194:117118. <https://doi.org/10.1016/J.APPLTHERMALENG.2021.117118>.
- Gao P, Wang LW, Zhu FQ. Vapor-compression refrigeration system coupled with a thermochemical resorption energy storage unit for a refrigerated truck. *Appl Energy May* 2021;290:116756. <https://doi.org/10.1016/J.APENERGY.2021.116756>.
- Verde M, Harby K, de Boer R, Corberán JM. Performance evaluation of a waste-heat driven adsorption system for automotive air-conditioning: Part I - Modeling and experimental validation. *Energy Dec*. 2016;116:526–38. <https://doi.org/10.1016/J.ENERGY.2016.09.113>.
- Shi B, Al-Dadah R, Mahmoud S, Elsayed A, Elsayed E. CPO-27(Ni) metal-organic framework based adsorption system for automotive air conditioning. *Appl Therm Eng Aug*. 2016;106:325–33. <https://doi.org/10.1016/J.APPLTHERMALENG.2016.05.109>.
- Freni A, Maggio G, Sapienza A, Frazzica A, Restuccia G, Vasta S. Comparative analysis of promising adsorbent/adsorbate pairs for adsorptive heat pumping, air conditioning and refrigeration. *Appl Therm Eng Jul*. 2016;104:85–95. <https://doi.org/10.1016/J.APPLTHERMALENG.2016.05.036>.
- Gao P, et al. Study on MnCl₂/CaCl₂-NH₃ two-stage solid sorption freezing cycle for refrigerated trucks at low engine load in summer. *Energy Convers Manag Feb*. 2016;109:1–9. <https://doi.org/10.1016/J.ENCONMAN.2015.11.055>.
- N. Yu, R. Z. Wang, and L. W. Wang, Sorption thermal storage for solar energy, *Progress in Energy and Combustion Science*, vol. 39, no. 5. Elsevier Ltd, pp. 489–514, 2013. doi: 10.1016/j.pecs.2013.05.004.
- G. An, L. Wang, Z. Wang, and J. Gao, Study on Working Pairs of Sorption Type Air Conditioner for Electric Vehicles under Different Temperature Zones, *Journal of Thermal Science* 2019 28:5, vol. 28, no. 5, pp. 1004–1014, Aug. 2019, doi: 10.1007/S11630-019-1132-6.
- Bao HS, Wang RZ, Oliveira RG, Li TX. Resorption system for cold storage and long-distance refrigeration. *Appl Energy May* 2012;93:479–87. <https://doi.org/10.1016/J.APENERGY.2011.12.022>.
- Ma Z, Bao H, Roskilly AP. Electricity-assisted thermochemical sorption system for seasonal solar energy storage. *Energy Convers Manag Apr*. 2020;209:112659. <https://doi.org/10.1016/J.ENCONMAN.2020.112659>.
- Thinsurat K, Bao H, Ma Z, Roskilly AP. Performance study of solar photovoltaic-thermal collector for domestic hot water use and thermochemical sorption seasonal storage. *Energy Convers Manag Jan*. 2019;180:1068–84. <https://doi.org/10.1016/J.ENCONMAN.2018.11.049>.
- Wu S, Li TX, Yan T, Wang RZ. Experimental investigation on a thermochemical sorption refrigeration prototype using EG/SrCl₂-NH₃ working pair. *Int J Refrig Apr*. 2018;88:8–15. <https://doi.org/10.1016/J.IJREFRIG.2017.11.030>.
- Jiang L, et al. Investigation on heat and mass transfer performance of novel composite strontium chloride for sorption reactors. *Appl Therm Eng Jul*. 2017;121: 410–8. <https://doi.org/10.1016/J.APPLTHERMALENG.2017.04.092>.
- Li TX, Wang RZ, Li H. Progress in the development of solid-gas sorption refrigeration thermodynamic cycle driven by low-grade thermal energy. *Prog Energy Combust Sci Feb*. 2014;40(1):1–58. <https://doi.org/10.1016/J.PECS.2013.09.002>.
- Ameen MT, Ma Z, Smallbone A, Norman R, Roskilly AP. Experimental study and analysis of a novel layered packed-bed for thermal energy storage applications: A proof of concept. *Energy Convers Manag Feb*. 2023;277:116648. <https://doi.org/10.1016/J.ENCONMAN.2022.116648>.
- Jung HS, Grady ML, Victoroff T, Miller AL. Simultaneously reducing CO₂ and particulate exposures via fractional recirculation of vehicle cabin air. *Atmos Environ Jul*. 2017;160:77–88. <https://doi.org/10.1016/J.ATMOSENV.2017.04.014>.
- Matysek M, et al. Optimising fen peatland water-table depth for romaine lettuce growth to reduce peat wastage under future climate warming. *Soil Use Manag Jan*. 2022;38(1):341–54. <https://doi.org/10.1111/SUM.12729>.
- Ma Z, Bao H, Roskilly AP. Seasonal solar thermal energy storage using thermochemical sorption in domestic dwellings in the UK. *Energy Jan*. 2019;166: 213–22. <https://doi.org/10.1016/J.ENERGY.2018.10.066>.
- H. Bao, Z. Ma, and A. P. Roskilly, Kinetic Models of Salt-Ammonia Chemisorption: An Overview and Comparison. Nova Science Publishers, 2018. Accessed: Apr. 11, 2023. [Online]. Available: <https://researchportal.hw.ac.uk/en/publications/kinetic-models-of-salt-ammonia-chemisorption-an-overview-and-comp>.
- Huang HJ, bin Wu G, Yang J, Dai YC, Yuan WK, Lu HB. Modeling of gas–solid chemisorption in chemical heat pumps. *Sep Purif Technol* 2004;34(1–3):191–200. [https://doi.org/10.1016/S1383-5866\(03\)00192-8](https://doi.org/10.1016/S1383-5866(03)00192-8).
- Kowsky C, Wolfe E, Leitzel L, Oddi F. Unitary HPAC System. *SAE Int J Passenger Cars Mech Syst Apr*. 2012;5(2):1016–25. <https://doi.org/10.4271/2012-01-1050>.
- Wu S, Li TX, Yan T, Wang RZ. Experimental investigation on a novel solid-gas thermochemical sorption heat transformer for energy upgrade with a large temperature lift. *Energy Convers Manag Sep*. 2017;148:330–8. <https://doi.org/10.1016/J.ENCONMAN.2017.05.041>.